ADSORPTION BEHAVIOUR OF METHYLENE BLUE ONTO NON-ACTIVATED DATE SEED BIOCHAR: KINETIC, EQUILIBRIUM, AND THERMODYNAMIC STUDIES

Atiqah Azhar, Nur Alyaa Insyirah Mohd Zamir, Zuliahani Ahmad, Abu Hassan Nordin*

Faculty of Applied Sciences, Universiti Teknologi MARA, Perlis, Malaysia

Received: 24 August 2026, Revised: 21 September 2026, Accepted: 22 September 2026, Published: 30 October 2026, Publisher: UTP Press, *Creative Commons: CC BY 4.0*
DOI: https://doi.org/10.61762/ijbrvol15iss2art2739

ABSTRACT

Methylene blue (MB) is a cationic dye that can persist in aquatic environments, requiring effective removal from contaminated water. In this study, non-activated date seed biochar (DSBC) was prepared through pyrolysis at 500°C and evaluated for MB adsorption from aqueous solution. N_2 adsorption–desorption analysis, Fourier Transform Infrared Spectroscopy (FTIR), and Field-Emission Scanning Electron Microscopy (FESEM) were used to characterise DSBC before and after adsorption. Following adsorption, the surface area and total pore volume decreased from 48.64 to 13.35 m^2/g and from 0.02376 to 0.010584 cm^3/g, respectively, indicating pore occupation by MB molecules. The highest MB removal efficiency, 94.75%, corresponding to an adsorption capacity of 9.475 mg/g, was obtained at a contact time of 5 min, an adsorbent dosage of 0.1 g, and a temperature of 90°C. The adsorption kinetics followed a pseudo-first-order model, whereas the equilibrium data fitted the Langmuir isotherm. Thermodynamic analysis indicated spontaneous, endothermic adsorption. Regeneration experiments demonstrated gradual decreases in removal efficiency from 94.7% to 50.2% over four cycles. These findings demonstrate the potential of non-activated DSBC for MB removal.

Keywords: *Biomass valorisation, pyrolysis, characterisations, dye wastewaters, regeneration, SDG 6, SDG 12*

INTRODUCTION

Water pollution is one of the world's most serious issues, primarily caused by the improper discharge of industrial waste, untreated sewage and wastewater, and rapid urban development. Among industrial sectors, the textile industry is one of the biggest contributors due to its high water consumption and extensive use of synthetic dyes across its production processes [1]. Globally, $\sim 7 \times 10^7$ tons of various dyes are manufactured annually, with more than 10,000 tons of synthetic dyes used in the textile industry [2]. These dye releases can cause toxic, mutagenic, and carcinogenic effects and may degrade the aesthetics of water bodies.

One such widely used synthetic dye is methylene blue (MB), known for its persistent, toxic, carcinogenic, and mutagenic properties [3]. Because of its remarkable stability and strong adherence to textile fibre, MB is frequently used as a colouring agent [4]-[5]. Structurally, MB is classified as a cationic dye since its molecule carries a permanent positive charge, namely the quaternary ammonium nitrogen in the thiazine ring. Exposure to MB has been associated with health problems such as vomiting [6], chest pain [7], and cancer [8]. MB poses a serious threat to aquatic ecosystems and organisms. For example, MB can be toxic to microalgae such as *Chlorella vulgaris* and *Spirulina platensis* by inhibiting their growth and protein content [9]. Thus, studies have focused on finding methods to eliminate synthetic dyes, especially MB, from wastewater.

Various techniques, such as membrane filtration [10], adsorption [11], and coagulation-flocculation [12], have been explored for dye removal from wastewater. Adsorption is a promising technique due to its high removal efficiency, ease of operation, and potential to use low-cost adsorbents. Various adsorbents have been investigated for MB removal, including activated carbon (AC) [13], composite adsorbents [14], and biomass-derived adsorbents [15]. Conventional AC is an excellent adsorbent for MB removal owing to its large surface area, well-developed pore structure, and favourable surface characteristics. Nevertheless, its production often requires additional activation steps, such as physical or chemical activation, which may consume significant energy or require an activating agent and subsequent washing. These requirements may increase production costs and generate additional environmental burdens, leading to growing interest in renewable and low-cost carbonaceous adsorbents derived from biomass residues. Biochar, a carbon-rich material produced via oxygen-limited thermochemical conversion of biomass (pyrolysis), has emerged as a promising alternative because of its porous structure and surface functional groups [16]. Furthermore, biochar manufacture from agricultural wastes offers a waste-to-wealth approach by reducing biomass waste and producing a value-added material for wastewater treatment.

Among various agricultural byproducts, *Phoenix dactylifera* (date) seeds (DS) are a promising carbonaceous precursor due to their lignocellulosic composition and carbon-rich structure. It has been

*Corresponding author.
E-mail address : abuhassannordin@uitm.edu.my

4 - IJBR 15(2)2026.indd 27 11/2/2026 11:07:48 AM

reported that DS contains 32.77% cellulose, 30.2% hemicellulose, and 37.03% lignin, which support carbon framework formation [17], while oxygen-containing groups (hydroxyl and carboxyl) may provide interaction sites for cationic MB. Recent studies have demonstrated the effectiveness of DS-derived materials in adsorbing dyes such as malachite green [18], Congo red [19], and MB [20], highlighting their suitability as renewable, low-cost adsorbents for wastewater treatment.

However, many studies on high-performance carbonaceous adsorbents have employed activation or surface modification to enhance their adsorption properties [21]-[23]. Therefore, further investigation is required to determine the adsorption potential of date seed biochar (DSBC) prepared via simple pyrolysis without chemical activation. More importantly, the relationship between the physicochemical characteristics of non-activated DSBC and its adsorption capacity for MB, particularly the changes occurring before and after adsorption, remains poorly understood. Therefore, this study aims to prepare and systematically characterise DSBC and to evaluate its adsorption performance for MB in aqueous solutions. The physicochemical properties of DSBC before and after MB adsorption were evaluated using Field Emission Scanning Electron Microscopy (FESEM), Fourier Transform Infrared Spectroscopy (FTIR), and N_2 adsorption–desorption analysis. Batch adsorption experiments were performed to assess the effect of the operating parameters on MB removal and to characterise the adsorption kinetics, isotherms, and thermodynamic parameters.

METHODOLOGY

Materials and Chemicals

The DS were acquired in the neighbourhood of Kuala Kangsar, Perak, Malaysia. The collected DS were used as the raw biomass feedstock for biochar production.

Preparation of Date Seed Biochar

The DS were thoroughly cleaned using distilled water to remove surface impurities and oven-dried at 90°C until a constant weight was attained. Then, these DS were pyrolysed in a muffle furnace at 500°C for 2 h at a heating rate of 10°C/min. The DSBC obtained after pyrolysis was left to cool to room temperature before being washed using distilled water to remove remaining ash and impurities. The dried DSBC was re-dried at 90°C for 1 h. Lastly, the DSBC was ground and sieved to a smaller particle size (<1 mm) for subsequent adsorption and characterisation studies.

Characterisation of Adsorbent

The DSBC were characterised using the following analytical methods to identify the structural changes before and after MB adsorption.

Fourier Transform Infrared Spectrometer

The functional groups of the DSBC both before and after MB adsorption were examined using FTIR. The analysis was performed using an FTIR spectrometer (IRTracer-100, Shimadzu Corporation, Japan) over the wavenumber range of 500–4000 cm^{-1} at a spectral resolution of 2 cm^{-1}. Approximately 0.01 g of each dried DSBC sample was finely ground and mixed with potassium bromide (KBr) at a 1:100 ratio. The mixture was thoroughly homogenised and compressed into a transparent pellet via a hydraulic press. The KBr pellet was then placed in the FTIR sample holder, and the resulting spectra were recorded for analysis.

Field Emission Scanning Electron Microscopy

FESEM was employed to characterise the DSBC surface morphology before and after MB adsorption. The characterisation was conducted utilising FESEM (Supra55VP, Carl Zeiss, Germany) at an accelerating voltage of 5 kV. Before analysis, each sample was placed onto an aluminium holder using double-sided carbon adhesive tape, then introduced to the FESEM chamber and examined at ×5,000 and ×10,000 magnifications.

Nitrogen Adsorption–Desorption Analysis

N_2 adsorption–desorption analysis was performed to quantify the specific surface area and pore volume of DSBC before and after MB adsorption. A Micromeritics 3Flex Surface Area Analyser (Micromeritics Instrument Corp., USA) was used to evaluate N_2 adsorption–desorption isotherms at 77 K. Before analysis, all samples were vacuum-degassed at 100°C for 3 h to remove moisture and any volatile impurities from the sample surface. The degassed samples were then analysed by N_2 adsorption–desorption analysis.

Batch Adsorption Experiments

Batch adsorption experiments were conducted with constant agitation at 120 rpm. The experiments followed the one-factor-at-a-time method, wherein a single parameter was varied while others remained constant, as summarised in Table 1. To ensure the reproducibility and validity of the results, all experiments were performed in triplicate. The MB dye concentrations before and after adsorption were measured using a HACH DR1900-01H portable spectrophotometer at a wavelength of 664 nm. A calibration curve with good linearity (coefficient of determination, $R^2 = 0.999$) was obtained using standard solutions of MB in the range of 0–10 mg/L. The calibration curve was subsequently used to calculate the MB residual following adsorption.

Table 1 Parameters varied in the adsorption study

Parameters	Variation
Effect of contact time (min)	3, 5,7,10, and 30
Effect of adsorbent dosage (g)	0.05, 0.1, 0.2, 0.3, and 0.5
Effect of temperature (°C)	27, 40, 60, 70, and 90

The MB dye percentage removal and adsorption capacity were determined using the following equations. Finally, all experiments will be performed in triplicate.

$$\text{Percentage removal (\%)} = \frac{C_o - C_f}{C_i} \times \quad (1)$$

4 - IJBR 15(2)2026.indd 28 11/2/2026 11:07:48 AM

$$\text{Adsorption capacity (qe)} = \frac{(C_o - C_f)V}{M} \quad (2)$$

where:
C_o and C_f (mg/L) = MB initial and final concentrations, V (L) is the total solution volume, and m (g) is the adsorbent dosage.

Model Fitting: Kinetic, Isotherm, and Thermodynamic Adsorption

Adsorption Kinetic Study

Adsorption kinetic modelling—pseudo-first-order (PFO), pseudo-second-order (PSO), and intraparticle diffusion (IPD) models—was utilised to understand the adsorption rate, the controlling mechanism, and the mass-transfer properties of MB onto the DSBC adsorbent. First, the PFO model describes the rate at which the adsorbate is adsorbed over time, where the rate of adsorption depends on the difference between the adsorbate concentration at any given time and its equilibrium concentration. The non-linear form of the PFO kinetic model is expressed as:

$$q_t = q_e(1 - e^{-k_1 t}) \quad (3)$$

where:
q_e and q_t (mg/g) = quantities of adsorbate uptake per mass of adsorbent at equilibrium and at a specific time, k_1 (1/ min) is the PFO equation's rate constant, and t is time (min).

Secondly, the PSO model states that the rate of adsorption is proportional to the quantity of adsorbate adsorbed onto the adsorbent surface, as well as to the amount adsorbed at equilibrium. The non-linear form of the PSO kinetic model is expressed as:

$$q_t = \frac{q_e^2 k_2 t}{1 + k_2 q_e t} \quad (4)$$

where:
q_e and q_t (mg/g) = quantities of adsorbate adsorbed per mass of adsorbent at equilibrium and at a particular time, k_2 (1/ min) PSO equation's rate constant, and t is time (min).

Finally, the IPD model describes the ability to transport adsorbate ions from solution into the adsorbent pores. The model is expressed as:

$$q_e = K_{id} t^{\frac{1}{2}} + C \quad (5)$$

where:
q_e (mg/g) = mass of dye adsorbed at time, K_{id} is the mass of adsorbate adsorbed at time (mg/g), and C denotes the y-intercept that indicates the boundary layer thickness.

Adsorption Isotherm Study

Adsorption isotherms describe the relationship between the MB solution concentration and the amount of MB adsorbed onto DSBC, providing insight into the adsorption mechanism, surface heterogeneity, and the characteristics of the adsorption layer. Langmuir and Freundlich models were used to analyse the adsorption data.

The Langmuir adsorption isotherm model was employed to analyse adsorption data from liquid solutions. It indicates that adsorption occurs on a surface with a limited number of uniform, equivalent sites, resulting in monolayer coverage. The non-linear Langmuir model is expressed as:

$$q_e = \frac{Q_{max} K_L C_e}{1 + K_L C_e} \quad (6)$$

where:
Q_{max} (mg/g) = maximum monolayer adsorption capacity,
C_e (mg/L) = concentration of adsorbate at equilibrium,
q_e (mg/g) = amount of adsorbate adsorbed at equilibrium, and
K_L (L/mg) = Langmuir constant related to adsorbate–adsorbent affinity.

Secondly, the Freundlich model explains the adsorption properties for a heterogeneous surface. The non-linear Freundlich is given as:

$$q_e = K_f C_e^n \quad (7)$$

where:
C_e (mg/L) = concentration of adsorbate at equilibrium,
1/n = heterogeneity factor,
q_e (mg/g) = amount of adsorbate adsorbed at equilibrium, and
K_f (mg/g)/(mg,/L) = Freundlich constant.

Adsorption Thermodynamic Study

Thermodynamic parameters such as Gibbs free energy change (ΔG°), enthalpy change (ΔH°), and entropy change (ΔS°) were utilised to evaluate the adsorption spontaneity process (endothermic or exothermic) as well as the degree of randomness at the adsorbate–adsorbent interface. The thermodynamic parameters were calculated as:

$$\Delta G° = -RT ln K_d \quad (8)$$

$$ln K_d = \frac{\Delta S°}{R} - \frac{\Delta H°}{RT} \quad (9)$$

where:
K_d = distribution coefficient (cm^3/g),
T = absolute temperature (Kelvin), and
R = gas constant (8.314 J/mol K).

Regeneration

Regeneration involves restoring spent adsorbents for reuse in subsequent adsorption cycles. Several regeneration methods have been studied, including thermal, chemical, and water-based regeneration. Thermal regeneration involves heating spent adsorbent to improve pollutant desorption, while chemical regeneration employs a chemical regenerant to desorb adsorbed pollutants from the adsorbent. Although these methods can restore adsorption capacity, they also require extra energy input or chemical reagents. In contrast, water-based regeneration offers

4 - IJBR 15(2)2026.indd 29 11/2/2026 11:07:49 AM

a simpler approach, using only distilled water, potentially reducing costs and minimising the risk of secondary pollution from the production and disposal of chemical waste.

In this study, MB adsorption onto DSBC was performed under optimal conditions. After adsorption, the spent DSBC was filtered from the dye solution, regenerated in distilled water for 30 min, and dried to a constant weight. The regenerated DSBC was then reused in subsequent adsorption cycles to evaluate its reusability. This adsorption-regeneration process was repeated until the MB removal efficiency fell below 50%.

RESULT AND DISCUSSION

Characterisation

These sections involved detailed characterisation of DSBC before and after MB adsorption using several analytical techniques like FTIR, FESEM, and N_2 adsorption–desorption analysis.

Functional Group and Structure Analysis

FTIR spectra were conducted to distinguish the functional groups present on the DSBC's surface before and after MB adsorption, as shown in Figure 1. Before adsorption, the DSBC exhibited several bands at 1573.25, 1190.40, and 740.39 cm^{-1}, assigned to aromatic C=C stretching, C-O stretching, and aromatic C-H bending vibrations, respectively. After MB adsorption, the bands were shifted to 1568.76, 1227.54, and 753.31 cm^{-1}. These changes suggest that the chemical environment of the hydroxyl, aromatic and C-O-containing groups was altered after MB adsorption.

New bands also appeared after MB adsorption at 3778.56 and 1702.96 cm^{-1}. The band at 3778.56 cm^{-1} can be assigned as a free O-H stretching vibration, which could be due to the presence of a hydroxyl group or adsorbed water on the surface of DSBC. Meanwhile, the 1702.96 cm^{-1} band may be ascribed to the C=O stretching vibration. Together, the peak shifts and appearance of new bands suggest changes in the surface chemistry of DSBC following MB uptake.

Surface Morphology of Adsorbent

The DSBC surface morphology before and after MB adsorption was analysed through FESEM. Before MB adsorption, DSBC exhibited a rough, irregular, and heterogeneous surface, with numerous pore openings (Figure 2a). These features result from the thermal decomposition of cellulose, hemicellulose, and lignin during pyrolysis, releasing volatile compounds and gases such as water vapour and carbon dioxide. The evolution of these gases creates voids and structural defects in the carbonaceous matrix, which provide accessible adsorption sites for MB molecules. Similar morphological structures have been reported for biochar derived from lignocellulosic precursors after pyrolysis, where thermal decomposition enhances the development of pore structures [24]-[25].

The surface morphology of the DSBC changed after MB adsorption, as depicted in Figure 2b. The MB-impregnated DSBC appeared relatively more heterogeneous, with MB deposits present within and around some of the pores, indicating MB deposition and accumulation on the DSBC surface. Similar observations have been reported for coconut-shell-derived biochar, where pores became

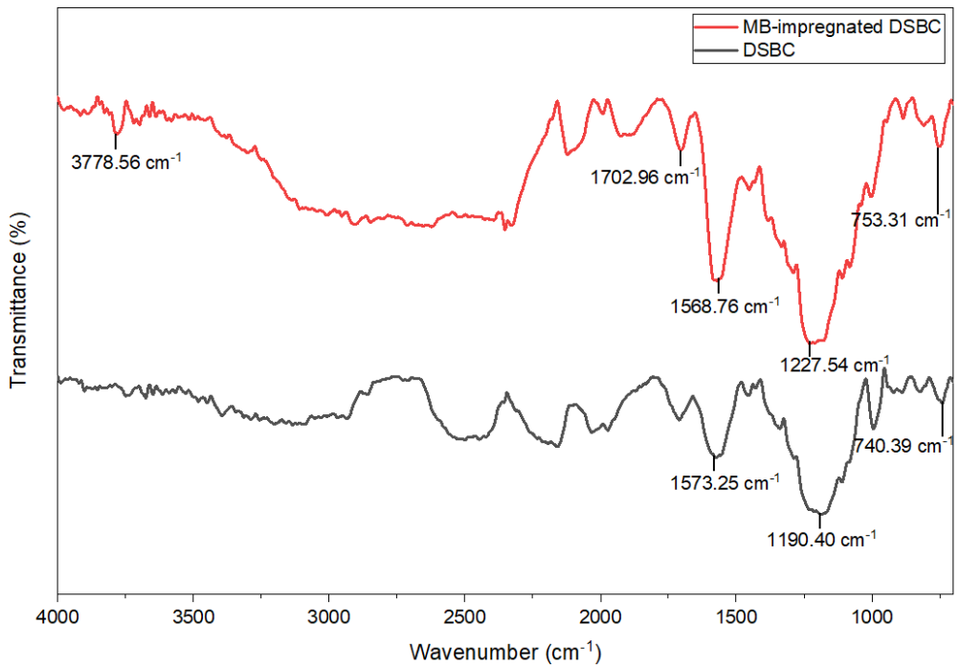

Figure 1 FTIR spectra of the DSBC before and after MB adsorption

4 - IJBR 15(2)2026.indd 30 11/2/2026 11:07:49 AM

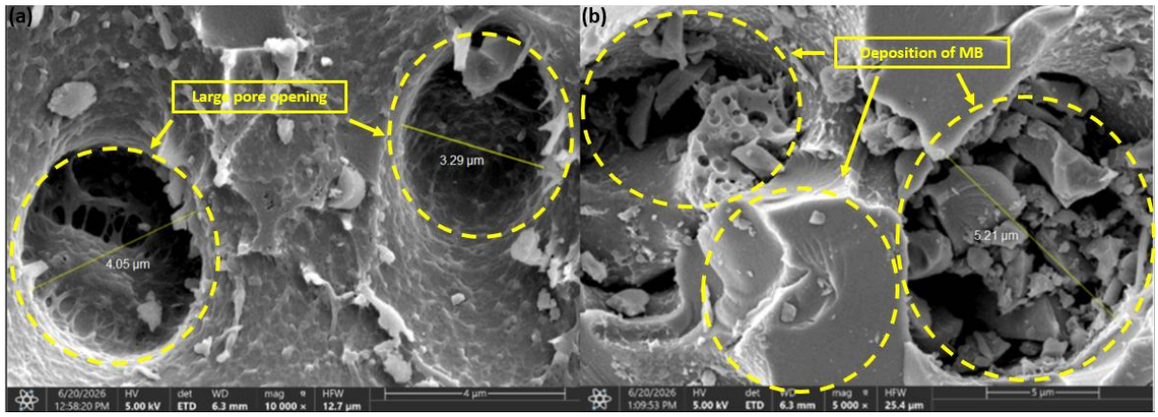

Figure 2 Surface morphology of DSBC (a) before and (b) after MB adsorption

partially filled after MB adsorption [26], supporting the findings for DSBC.

Large surface openings were identified on the DSBC with apparent dimensions of 3.29 and 4.05 µm. After MB adsorption, a representative pore opening had an apparent dimension of 5.21 µm. An increase in the apparent dimensions after MB adsorption does not necessarily indicate an enlargement of the original pore structure. Rather, it can be correlated with the changes in surface morphology caused by the deposition and possible aggregation of MB molecules on the DSBC's surface. It has been reported that dye adsorption onto biochar leads to surface agglomeration, pore blockage, and dye deposition on the biochar surface, thereby altering its surface properties [27]. Therefore, the dimensions measured in this study represent the apparent dimensions of certain surface openings in two-dimensional FESEM images, rather than direct measurements of the three-dimensional pore network.

Surface Area, Pore Size, and Pore Volume of Adsorbent

The surface area and pore properties of DSBC before and after MB adsorption were measured using N_2 adsorption–desorption analysis. The N_2 adsorption–desorption analysis of DSBC, as in Figure 3a, showed a constant increase in N_2 uptake at low relative pressure, followed by a more gradual increase over the intermediate relative pressure range (P/P_o = 0.1–0.8). The gradual uptake at intermediate P/P_o is associated with multilayer adsorption and capillary condensation within mesopores, while further increase in N_2 uptake at higher P/P_o indicates further filling of the accessible pore network and interparticle voids [28]. The presence of a hysteresis loop between the adsorption and desorption branches represents Type IV isotherms with an H3-type hysteresis loop, suggesting the presence of mesopores. This feature indicates that DSBC has a heterogeneous porous structure with various accessible pore sizes.

After MB adsorption, the N_2 adsorption–desorption isotherm of MB-impregnated DSBC, as shown in Figure 3b, also showed Type IV characteristics with a similar hysteresis behaviour. However, the N_2 uptake was lower than that of DSBC across most parts of the relative pressure range. At lower P/P_o (<0.1), the MB-impregnated DSBC showed an initial increase in N_2 uptake, while a gradual increase was observed at intermediate P/P_o. The lower N_2 uptake after MB adsorption suggested that the pore network became less accessible, indicating the occupation or partial blockage of accessible pores by MB, thereby limiting the diffusion of N_2 molecules into pores during the analysis [29]. This observation is further supported by textural properties determined from N_2 adsorption–desorption analysis. The DSBC showed a specific surface area and total pore volume of 48.64 $m^2 g^{-1}$ and 0.02376 $cm^3 g^{-1}$, respectively. After MB adsorption, the specific surface area and total pore volume decreased to 13.35 $m^2 g^{-1}$ and 0.010584 $cm^3 g^{-1}$, respectively. These decreases suggested that some of the surface areas and pores became inaccessible to N_2 molecules. Similar reductions in specific surface area and pore volume have also been reported after dye adsorption onto biochar-based adsorbents, which was correlated with the occupation of accessible pores with dye molecules [30]-[31].

The pore size distribution shown in Figure 3c illustrates the pore structure after MB adsorption. The pore widths in both samples showed a wide distribution; pore volume was greater at smaller pore widths and decreased gradually towards larger pore widths. After MB adsorption, the contribution to pore volume at smaller pore widths was reduced, indicating that some of the smaller pores were occupied or partially blocked by MB molecules. This is consistent with the decrease in specific surface area and total pore volume, as the occupation of the smaller pores reduced their contribution to the accessible pore network.

The average pore diameter increased from 1.95 to 3.17 nm, respectively. This increase should not be interpreted as the physical enlargement of the DSBC pores. Instead, it can be attributed to a decrease in the contribution from smaller pores after binding or partial blockage by MB molecules. Consequently, the reduction in specific surface area and pore volume along with an increase in average pore diameter does not necessarily indicate that larger pores are formed during MB adsorption; rather, it reflects a change in the pore accessibility and pore size distribution.

4 - IJBR 15(2)2026.indd 31 11/2/2026 11:07:49 AM

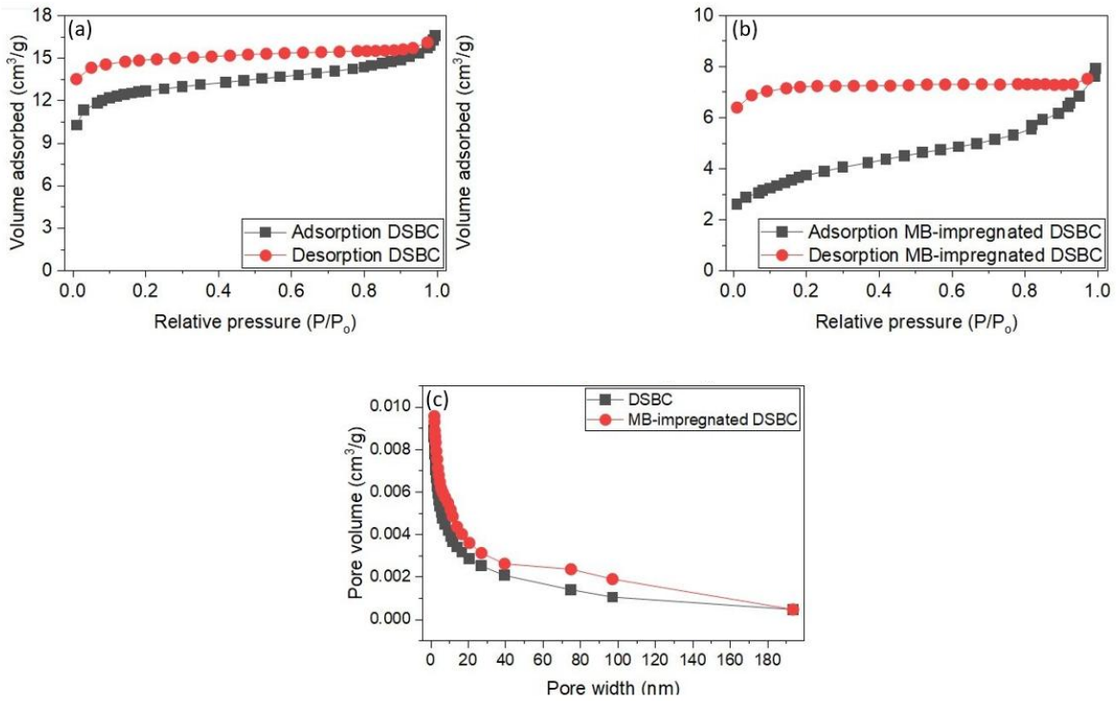

Figure 3 Nitrogen adsorption–desorption isotherms of (a) DSBC, (b) MB-impregnated DSBC, (c) pore size distribution of DSBC and MB-impregnated DSBC

Effect of Adsorption Parameters

The adsorption of MB onto the DSBC was investigated through three parameters: contact time, adsorbent dosage, and temperature.

Effect of Contact Time

The effect of contact time on MB removal by DSBC was studied from 3 to 30 min, as illustrated in Figure 4. At the initial stage,

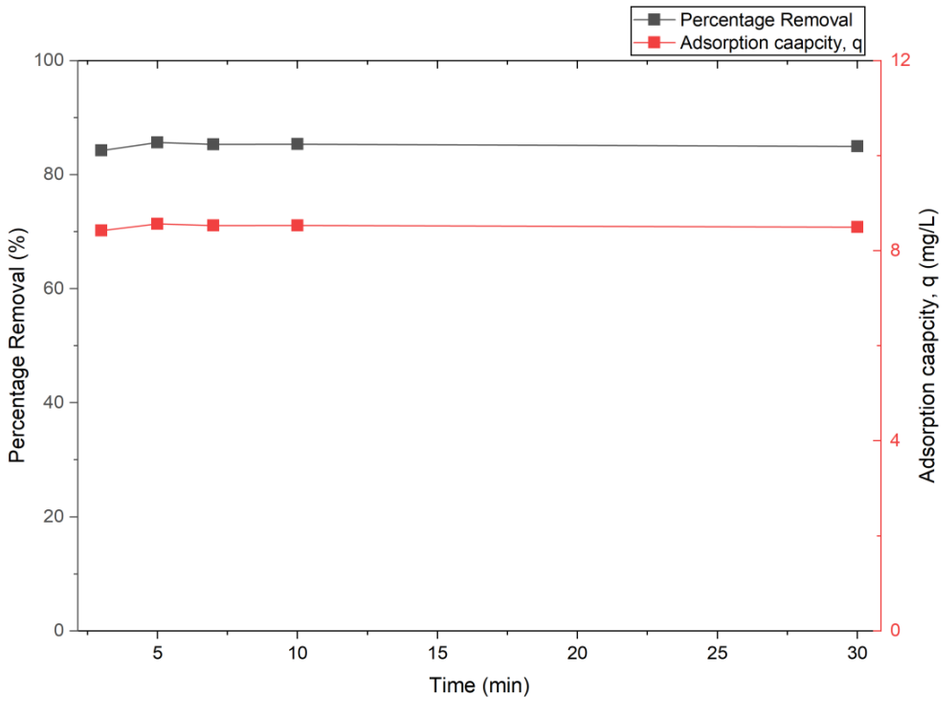

Figure 4 Effect of contact time on the removal of MB

4 - IJBR 15(2)2026.indd 32 11/2/2026 11:07:50 AM

rapid adsorption occurred, with 84.23% (8.423 mg/g) of MB being removed within the first 3 min. This rapid uptake was attributed to the high availability of active sites on the DSBC surface, which facilitated the rapid adsorption of MB molecules [32]. At 5 min, the removal efficiency increased to 85.65% and slightly increased to 87.26% at 30 min. This limited increase suggests a transition from rapid to slower adsorption. This is because most readily accessible adsorption sites were already occupied during the initial stage, leaving fewer sites available for subsequent adsorption. Hence, 5 min was selected as the optimal contact time, as high MB removal efficiency was achieved within this short duration.

Effect of Adsorbent Dosage

The effect of adsorbent dosage on the MB removal efficiency and adsorption capacity was evaluated, as illustrated in Figure 5. As the adsorbent dosage increased (from 0.05 to 0.10 g), the MB removal efficiency increased from 77.32 to 85.65%. This improvement was due to increased availability of active sites, which provided additional sites for MB molecules to adsorb. With a further increase in adsorbent dosage (from 0.20 to 0.50 g), the removal efficiency increased slightly from 86.34% to a maximum of 89.40%. The relatively small improvement at the higher adsorbent dosage indicates that most readily available MB molecules had already been adsorbed, resulting in only a slight increase in MB removal.

In contrast, the adsorption capacity decreased from 15.464 to 8.565 mg/g with increasing adsorbent dosage. This reduction resulted from a greater number of adsorption sites relative to the fixed quantity of MB in solution, leading to a decrease in MB adsorption capacity. Hence, 0.10 g was selected as the optimal adsorbent dosage due to its high removal efficiency and adsorption capacity.

Effect of Temperature

The MB removal efficiency and adsorption capacity increase slightly with increasing temperature (from 25 to 40°C), then rise significantly upon reaching 90°C, as depicted in Figure 6. The maximum removal efficiency and adsorption capacity were obtained at 90°C with values of 94.75% and 9.475 mg/g. These increases suggest an endothermic adsorption process. The higher kinetic energy of MB molecules might account for this improvement, as it promotes their diffusion toward adsorption sites in DSBS pores. Furthermore, higher temperatures decrease the solution's viscosity, thereby increasing the mobility and diffusion of MB molecules through the adsorbent pores [23]. Besides, higher temperatures may reduce the mass-transfer resistance at the adsorbent boundary layer, facilitating the movement of MB molecules from the bulk solution toward the DSBC's surface.

Adsorption Modelling

To better understand the adsorption mechanism, the adsorption kinetics, isotherms, and thermodynamic reactions were carefully evaluated.

Adsorption Kinetic

The adsorption kinetic studies were conducted using PFO, PSO, and

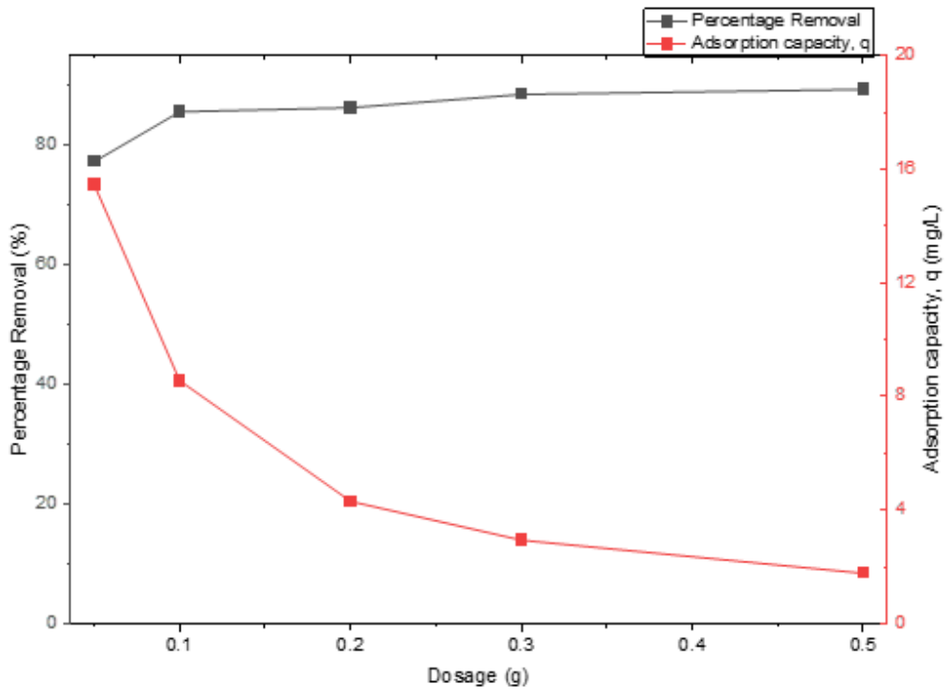

Figure 5 Effect of adsorbent dosage on the removal of MB

4 - IJBR 15(2)2026.indd 33 11/2/2026 11:07:50 AM

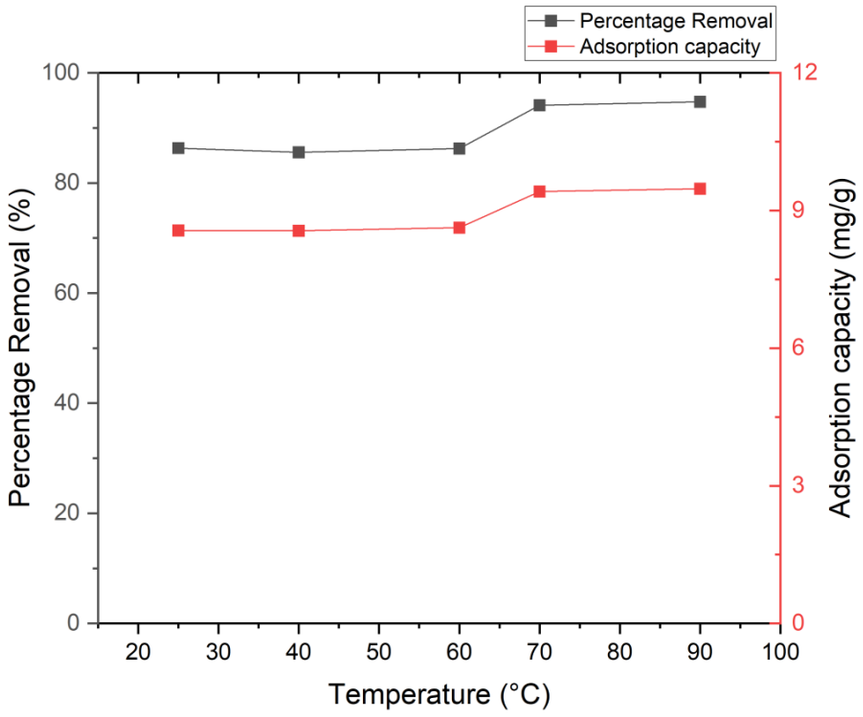

Figure 6 Effect of temperature on the removal of MB

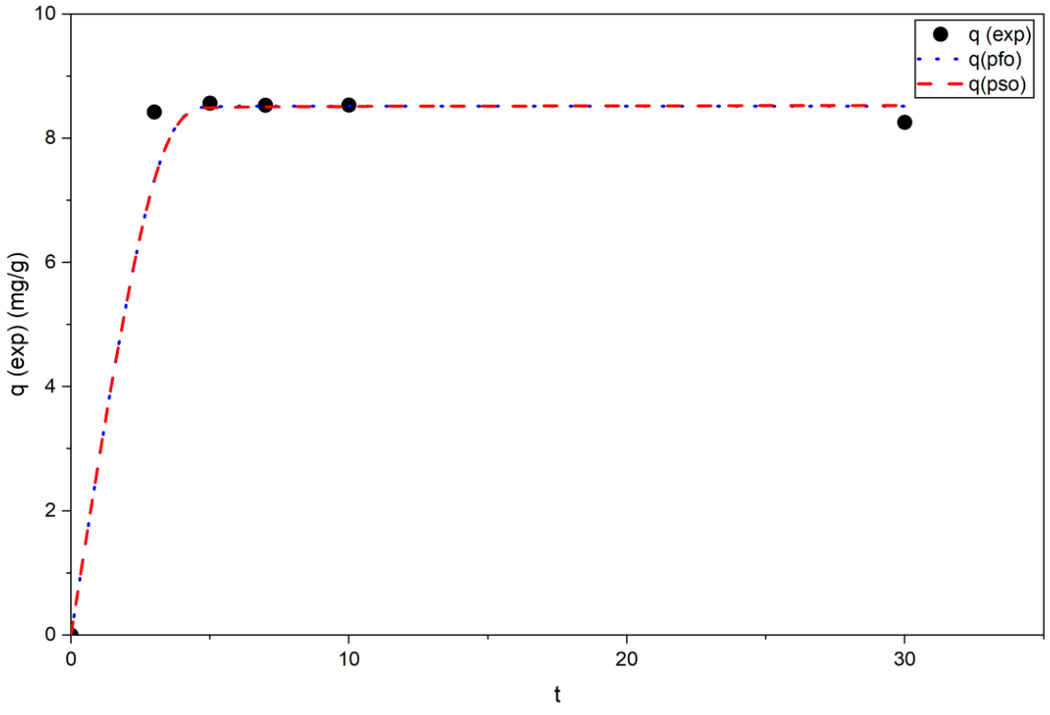

Figure 7 PFO and PSO kinetic models for MB adsorption onto DSBC

4 - IJBR 15(2)2026.indd 34 11/2/2026 11:07:50 AM

IPD models to assess the kinetics of MB adsorption by DSBC and investigate the possible rate-controlling mechanism of adsorption. The non-linear plots for the PFO and PSO models are presented in Figure 7.

The PFO and PSO kinetic parameters are illustrated in Table 2. The most suitable kinetic model was selected based on the linear correlation coefficient (R^2) and the lowest analysis error function (χ^2) value [33]. Both models show high R^2 values, indicating good agreement with experimental results. Nevertheless, the PFO model showed a slightly higher linear coefficient of determination (R^2 = 0.9988) than the PSO model (R^2 = 0.9986). In addition, the PFO model also had a lower value of the error function (χ^2 = 0.00847) than the PSO model (χ^2 = 0.00965). Hence, the PFO model demonstrated a slightly better fit to the experimental results compared to the PSO model. These results demonstrate that the adsorption kinetics of MB onto the DSBC depend primarily on the availability and progressive occupation of adsorption sites, especially during the rapid initial stage of adsorption.

Table 2 Adsorption rate constants for MB adsorption onto DSBC

Kinetic model	MB value
PFO	
k_1 (1/min)	1.6821
qe (calc) (mg/g)	8.5160
χ^2	0.00847
R^2	0.9988
PSO	
K^2 (1/min)	4.6842
Q_e (calc) (mg/g)	8.5360
χ^2	0.00965
R^2	0.9986

The IPD model was applied to identify the possible diffusion mechanism of DSBC. As shown in Figure 8, the adsorption process involved two stages. The first stage corresponds to the rapid uptake of MB, driven by the diffusion of MB molecules from the bulk solution to the external surface of biochar [34]. The second stage represents a slower adsorption process that occurred due to the progressive diffusion of MB molecules into the internal pores of the biochar and the reduction in available adsorption sites [34].

Isotherm Kinetics

The Langmuir and Freundlich adsorption models were utilised to assess the applicability of the adsorption isotherm, as depicted in Figure 9. The R^2 value obtained from the Langmuir and Freundlich isotherm models were 0.9044 and 0.6880. The higher obtained R^2 value for Langmuir suggests that it provided a better fit to the experimental equilibrium data than the Freundlich model. Therefore, the Langmuir model was found to be more suited to describe the equilibrium adsorption of MB by DSBC.

Thermodynamic Modelling

The thermodynamic parameters for MB adsorption onto DSBC were calculated over the temperature range 298-363 K, as shown in Figure 10 and Table 3. At the temperatures investigated, ΔG° values were negative, ranging from −21.119 to −29.289 kJ/mol. These negative ΔG° values suggest that the MB adsorption process by DSBC was thermodynamically spontaneous. In addition, the ΔG° value became more negative as temperature increased, indicating that the adsorption process was thermodynamically favoured at higher temperatures. This trend is consistent with the experimental finding that MB adsorption capacity increases with temperature. The positive ΔH° value (16.3580 kJ/mol) indicates that adsorption is endothermic, with heat absorbed during adsorption. The positive

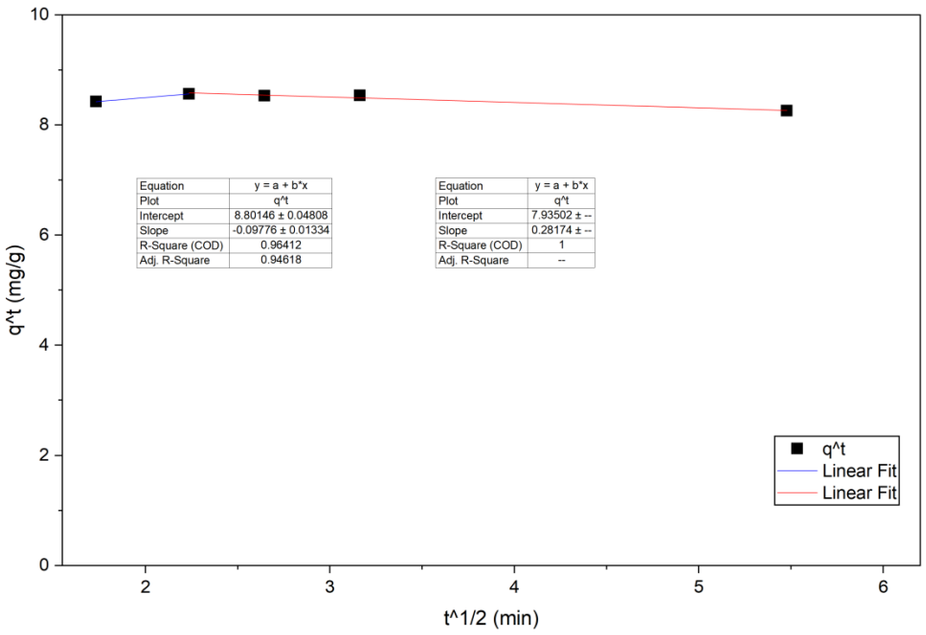

Figure 8 IPD model of MB adsorption onto DSBC

4 - IJBR 15(2)2026.indd 35 11/2/2026 11:07:50 AM

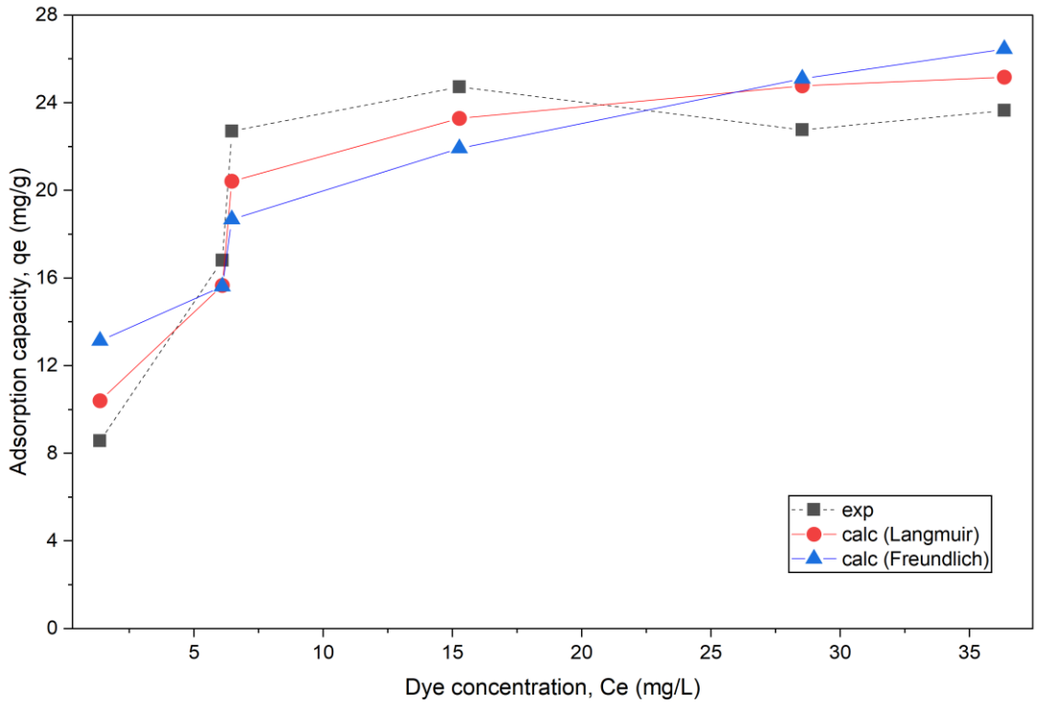

Figure 9 Adsorption isotherms of Langmuir and Freundlich for DSBC

ΔS° value of 125.6987 J/ mol. K describes the increase in randomness at the adsorbent–solution interface during adsorption. Overall, MB adsorption on DSBC was spontaneous and endothermic, with the adsorption becoming more favourable as temperature increased.

Regeneration Performance of DSBC

The regeneration performance of DSBC was assessed over four consecutive adsorption-regeneration cycles, as shown in Figure 11. DSBC showed a removal efficiency of 94.7% in the first cycle,

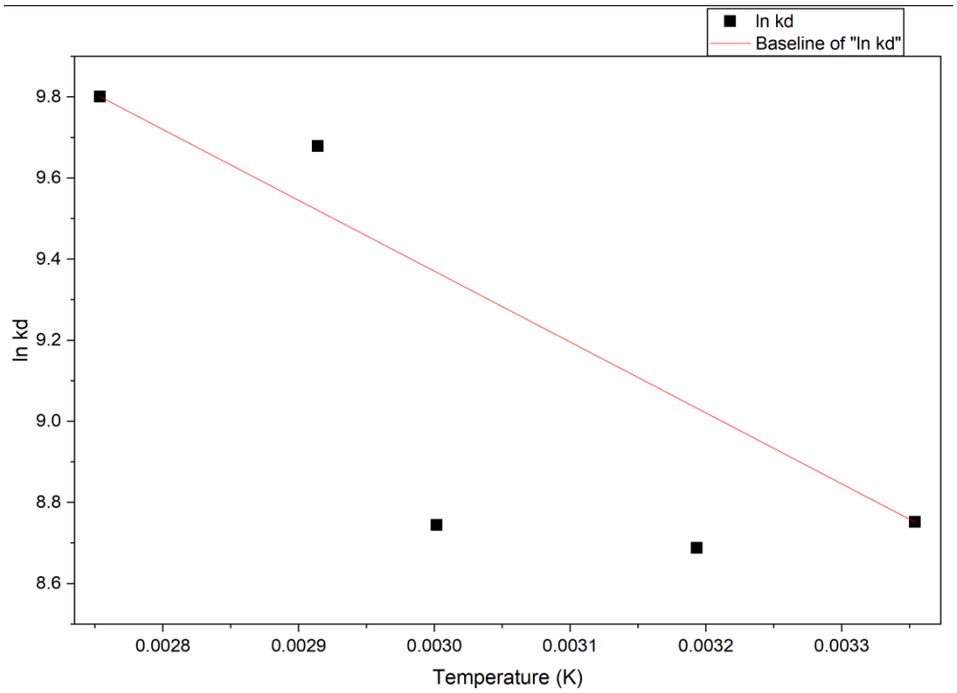

Figure 10 Thermodynamic plot for MB adsorption onto DSBC

4 - IJBR 15(2)2026.indd 36 11/2/2026 11:07:50 AM

Table 3 Thermodynamic parameters of MB dye adsorption onto DSBC

Temperature (K)	Thermodynamic parameters			
	ln Kd	ΔG (kJ/mol)	ΔH (kJ/mol)	ΔS (J/mol. K)
298	8.743	−21.119		
313	8.688	−23.004		
333	8.744	−25.518	16.3580	125.6987
343	9.679	−26.775		
363	9.801	−29.289		

indicating that the adsorbent maintained high MB removal performance. The removal efficiency decreased to 82.3%, 65.9%, and 50.2% in the second, third, and fourth cycles. This progressive reduction in MB removal could be due to incomplete desorption of MB during regeneration, leaving residual dye molecules on the surface or within the DSBC pore structure. Therefore, DSBC shows potential for reuse in repeated adsorption-regeneration cycles for wastewater treatment.

CONCLUSIONS

DSBC was successfully prepared via pyrolysis at 500°C and showed potential for MB removal from aqueous solution. The optimal removal efficiency and adsorption capacity were achieved at 94.75% and 9.475 mg/g, respectively, under the optimal conditions of 5 min contact time, 0.1 g DSBC, and 90°C. The adsorption kinetics followed the PFO model, while the Langmuir model best represented the equilibrium data. Thermodynamic analysis showed that the adsorption process was endothermic and favourable at higher temperatures. Regeneration experiments indicated that the DSBC remained stable over four cycles, with the removal efficiency decreasing from 94.7% to 50.2%. Overall, DSBC shows potential as a sustainable adsorbent for dye wastewater treatment.

CONFLICT OF INTEREST

The authors declare that they have no known competing financial interests or personal relationships that could have appeared to influence the work reported in this paper.

ACKNOWLEDGMENT

The authors sincerely appreciate the Ministry of Higher Education (MoHE) Malaysia for funding support through the Fundamental Research Grant Scheme (FRGSEC/1/2024/WAS02/UITM/02/15).

AUTHORS' CONTRIBUTION

Atiqah Azhar conceptualised and drafted the manuscript. Nur Alyaa Insyirah Mohd Zamir collected and analysed the data. Zuliahani Ahmad reviewed and edited the manuscript critically for intellectual content. Abu Hassan Nordin supervised the project, provided resources, secured funding, and validated the concept and content. All authors have read and approved the final version of the manuscript.

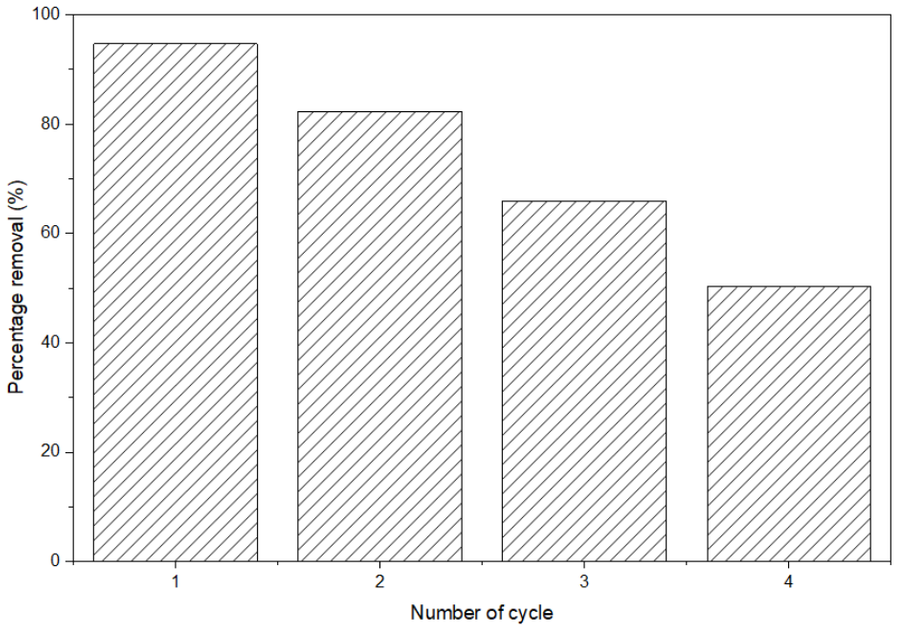

Figure 11 The regeneration cycle of DSBC

4 - IJBR 15(2)2026.indd 37 11/2/2026 11:07:50 AM

REFERENCES

[1] R. Al-Tohamy, S. S. Ali, F. Li, K. M. Okasha, Y. A.-G. Mahmoud, T. Elsamahy, H. Jiao, Y. Fu, and J. Sun, "A critical review on the treatment of dye-containing wastewater: Ecotoxicological and health concerns of textile dyes and possible remediation approaches for environmental safety," *Ecotoxicology and Environmental Safety*, vol. 231, p. 113160, 2022, doi: 10.1016/j.ecoenv.2021.113160.

[2] R. Kishor, D. Purchase, G. D. Saratale, R. G. Saratale, L. F. R. Ferreira, M. Bilal, R. Chandra, and R. N. Bharagava, "Ecotoxicological and health concerns of persistent coloring pollutants of textile industry wastewater and treatment approaches for environmental safety," *Journal of Environmental Chemical Engineering*, vol. 9, no. 2, p. 105012, 2021, doi: 10.1016/j.jece.2020.105012.

[3] P. O. Oladoye, T. O. Ajiboye, E. O. Omotola, and O. J. Oyewola, "Methylene blue dye: Toxicity and potential elimination technology from wastewater," *Results in Engineering*, vol. 16, p. 100678, 2022, doi: 10.1016/j.rineng.2022.100678.

[4] T. Saeed et al., "Synthesis of chitosan composite of metal-organic framework for the adsorption of dyes; kinetic and thermodynamic approach," *Journal of Hazardous Materials*, vol. 427, p. 127902, 2022, doi: 10.1016/j.jhazmat.2021.127902.

[5] X.-J. Liu, M.-F. Li, and S. K. Singh, "Manganese-modified lignin biochar as adsorbent for removal of methylene blue," *Journal of Materials Research and Technology*, vol. 12, pp. 1434–1445, 2021, doi: 10.1016/j.jmrt.2021.03.076.

[6] A. Yaqub, M. Zahid, M. U. Nisa, T. Iqbal, K. H. Shah, N. S. Shah, and M. U. Draz, "Sustainable removal of methylene blue dye from textile effluents by magnetised tea waste and peanut shells," *Chemical Engineering Science,* vol. 299, p. 120498, 2024, doi: https://doi.org/10.1016/j.ces.2024.120498.

[7] M. Bužga, E. Machytka, E. Dvořáčková, Z. Švagera, D. Stejskal, J. Máca, and J. Král, "Methylene blue: a controversial diagnostic acid and medication?," *Toxicol. Res. (Camb.)*, vol. 11, no. 5, pp. 711–717, 2022, doi: 10.1093/toxres/tfac050.

[8] A. Seitkazina, J.-K. Yang, and S. Kim, "Clinical effectiveness and prospects of methylene blue: A systematic review," *Precision and Future Medicine*, vol. 6, no. 4, pp. 193–208, 2022, doi: 10.23838/pfm.2022.00079.

[9] A. Krishna Moorthy, B. Govindarajan Rathi, S. P. Shukla, K. Kumar, and V. Shree Bharti, "Acute toxicity of textile dye Methylene blue on growth and metabolism of selected freshwater microalgae," *Environmental Toxicology and Pharmacology*, vol. 82, p. 103552, 2021, doi: 10.1016/j.etap.2020.103552.

[10] J. E. Cevallos-Mendoza, C. Amorim, J. Rodríguez-Díaz, and M. Montenegro, "Removal of contaminants from water by membrane filtration: a review," *Membranes*, vol. 12, p. 570, 2022, doi: 10.3390/membranes12060570.

[11] N. Ali, N. Jabbar, S. Mohsen, H. Majdi, and T. Albayati, "Adsorption of methyl violet dye onto a prepared bio-adsorbent from date seeds: isotherm, kinetics, and thermodynamic studies," *Heliyon*, vol. 8, p. e10276, 2022, doi: 10.1016/j.heliyon. 2022.e10276.

[12] C. Zaharia, M. Petronela, and M.-A. Afrasinei, "The use of coagulation–flocculation for industrial colored wastewater treatment—(I) the application of hybrid materials," *Applied Sciences*, vol. 14, p. 2184, 2024, doi: 10.3390/app14052184.

[13] H. Jedli, S. M. Bouzgarrou, R. Hassani, E. Sabi, L. Jamel, and K. Slimi, "Adsorption mechanisms of methylene blue and methyl orange on activated carbon: Scientific interpretation and modeling simulation," *Scientific Reports*, vol. 16, no. 1, p. 26809, 2026, doi: 10.1038/s41598-026-52640-2.

[14] D. Rao Vaddi, R. Malla, and S. Geddapu, "Magnetic activated carbon: A promising approach for the removal of methylene blue from wastewater," *Desalination and Water Treatment*, vol. 317, p. 100146, 2024, doi: 10.1016/j.dwt.2024.100146.

[15] M. Chanie Shumie, H. Hailu, and E. Alemayehu, "Turning Prosopis juliflora invasive biomass into a sustainable adsorbent: Mechanistic and reusability studies for methylene blue removal," *Results in Surfaces and Interfaces*, vol. 23, p. 100797, 2026, doi: 10.1016/j.rsurfi.2026.100797.

[16] Y. Zhang, H. Chen, and S. Islam, "Advances in biochar modification for environmental remediation with emphasis on iron functionalisation," *Biochar X*, vol. 1, 2025, doi: 10.48130/bchax-0025-0010.

[17] G. Albornoz-Palma, D. Ching, O. Valerio, R. Mendonça, and M. Pereira, "Effect of lignin and hemicellulose on the properties of lignocellulose nanofibril suspensions," *Cellulose*, vol. 27, 2020, doi: 10.1007/s10570-020-03304-5.

[18] F. H. Sorour, N. M. Aboeleneen, N. M. Abd El-Monem, Y. A. Ammar, and R. A. Mansour, "Removal of malachite green from wastewater using date seeds as natural adsorbent; isotherms, kinetics, Thermodynamic, and batch adsorption process design," *International Journal of Phytoremediation*, vol. 26, no. 8, pp. 1321–1335, 2024, doi: 10.1080/15226514.2024.2316315.

[19] R. T. Kapoor, M. Rafatullah, H. A. Tajarudin, M. R. Siddiqui, and M. Alam, "Treatment of Direct Red 28 Dye through Phoenix dactylifera L. Fruit Seed Biochar: Equilibrium, Kinetics, Thermodynamics, and Phytotoxicity Studies," *Sustainability*, vol. 15, no. 21, p. 15266, 2023, doi: 10.3390/su152115266.

4 - IJBR 15(2)2026.indd 38 11/2/2026 11:07:50 AM

[20] A. D. Alsulaili, A. A. Refaie, and H. A. Garcia, "Adsorption capacity of activated carbon derived from date seeds: Characterisation, optimisation, kinetic and equilibrium studies," *Chemosphere*, vol. 313, p. 137554, 2023, doi: 10.1016/j.chemosphere.2022.137554.

[21] S. Khaleefa Ali and H. Hamad, "Textile dye removal by activated date seeds," *Engineering and Technology Journal*, vol. 37, pp. 242–247, 2019, doi: 10.30684/etj.37.2C.7.

[22] A. Ouedrhiri, M. Ait Himi, B. Youbi, Y. Lghazi, J. Bahar, C. El Haimer, A. Aynaou, and I. Bimaghra, "Biochar material derived from natural waste with superior dye adsorption performance," *Materials Today: Proceedings*, vol. 66, pp. 259–267, 2022, doi: 10.1016/j.matpr.2022.04.928.

[23] R. Fath Allah, H. Ouaddari, J. Hernández-Saz, I. El Fellah, A. Fakih Lanjri, D. Goma Jiménez, J. Bensalah, and M. Ouzzine, "Activated carbon derived from palm date seeds as an adsorbent for methylene blue: kinetic and thermodynamic studies," *Reaction Kinetics, Mechanisms and Catalysis*, vol. 137, no. 6, pp. 3343–3364, 2024, doi: 10.1007/s11144-024-02710-1.

[24] S. Somboon, S. Schlichenmaier, K. Thumanu, P. Pakawanit, S. Yodda, T.-S. Sukitprapanon, and P. Lawongsa, "Transformations in physicochemical properties and pore structure of biochar derived from rice straw revealed by synchrotron techniques," *Scientific Reports*, vol. 15, no. 1, p. 23641, 2025, doi: 10.1038/s41598-025-08772-y.

[25] H. Tian, Y. Wei, S. Cheng, Z. Huang, M. Qing, Y. Chen, H. Yang, and Y. Yang, "Optimising the gasification reactivity of biochar: The composition, structure and kinetics of biochar derived from biomass lignocellulosic components and their interactions during gasification process," *Fuel*, vol. 324, p. 124709, 2022, doi: 10.1016/j.fuel.2022.124709.

[26] D. Nuryana, M. F. R. Alim, M. Yahayu, M. A. A. Zaini, R. S. R. Sulong, M. F. S. Abd Aziz, H. Prasetiawan, Z. A. Zakaria, and R. D. Kusumaningtyas, "Methylene blue removal using coconut shell biochar synthesised through microwave-assisted pyrolysis," *Jurnal Teknologi (Sciences & Engineering)*, vol. 82, no. 5, 2020, doi: 10.11113/jt.v82.14359.

[27] J. Wang, Y. Tan, H. Yang, L. Zhan, G. Sun, and L. Luo, "On the adsorption characteristics and mechanism of methylene blue by ball mill modified biochar," *Scientific Reports*, vol. 13, no. 1, p. 21174, 2023, doi: 10.1038/s41598-023-48373-1.

[28] M. W. U. Zaman, A. D. Phule, T. G. Senthamaraikannan, S. Y. Kim, S. Elkaee, J. H. Yang, and D.-H. Lim, "Design of bifunctional nitrogen-doped biochar with adsorption and catalytic oxidation capabilities for enhanced toluene emission control," *Environmental Research*, vol. 269, p. 120867, 2025, doi: 10.1016/j.envres.2025.120867.

[29] M. Kashif, C. Kang, A. Ranjbari, Y. Su, and P. M. Heynderickx, "Interaction of rhodamine B with porous clay heterostructures: Integrating structural changes, kinetics, and isotherm study," *Vacuum*, vol. 245, p. 115000, 2026, doi: 10.1016/j.vacuum.2025.115000.

[30] K. Abdullah and S. Hadi Ahmed, "Sustainable removal of methylene blue from water using a chitosan/date-pit biochar composite: Adsorption behavior and environmental implications," *Journal of Ecological Engineering*, vol. 27, pp. 206–221, 2026, doi: 10.12911/22998993/218700.

[31] S. Fersiz, M. Isgoren, E. Gengec, and S. Demir, "Optimisation of sustainable hybrid natural–waste adsorbent compositions for mixed dye removal from aqueous solutions," *Water, Air, & Soil Pollution*, vol. 237, no. 11, p. 627, 2026, doi: 10.1007/s11270-026-09300-y.

[32] H. Hadda Aya, N. Djamel, A. Samira, M. Otero, and M. Ali Khan, "Optimising methylene blue adsorption conditions on hydrothermally synthesised NaX zeolite through a full two-level factorial design," *RSC Adv*, vol. 14, no. 33, pp. 23816–23827, 2024, doi: 10.1039/d4ra04483e.

[33] B. Saawarn, B. Mahanty, and S. Hait, "Adsorption of perfluorooctanoic acid from aqueous matrices onto chitosan-modified magnetic biochar: Response surface methodology-based modeling, performance, and mechanism," *Environmental Pollution*, vol. 368, p. 125734, 2025, doi: 10.1016/j.envpol.2025.125734.

[34] F. Bu, L. Han, H. Guo, Y. Liang, and H. Yan, "Unraveling the synergistic mechanisms of phosphorus adsorption and slow-release on low-Mg-loaded biochar enabled by KOH activation," *Materials*, vol. 18, no. 22, p. 5214, 2025, doi: 10.3390/ma18225214.

4 - IJBR 15(2)2026.indd 39 11/2/2026 11:07:51 AM